Magnetic domains in epitaxial $BaFe_{12}O_{19}$ thin films with perpendicular anisotropy

2002 J. Phys.: Condens. Matter 14 12339

(http://iopscience.iop.org/0953-8984/14/47/309)

INSTITUTE OF PHYSICS PUBLISHING JOURNAL OF PHYSICS: CONDENSED MATTER

J. Phys.: Condens. Matter **14** (2002) 12339–12352 PII: S0953-8984(02)39104-5

Magnetic domains in epitaxial $BaFe_{12}O_{19}$ thin films with perpendicular anisotropy

A Lisfi[1,2,3] **and J C Lodder**[1]

[1] SMI, MESA+ Research Institute, University of Twente, PO Box 217, 7500 AE Enschede, The Netherlands
[2] Morgan State University, Department of Physics, 1700 E. Cold Spring Lane, Baltimore, MD 21251, USA

E-mail: alisfi@jewel.morgan.edu

Received 4 July 2002
Published 15 November 2002
Online at stacks.iop.org/JPhysCM/14/12339

Abstract

Magnetic domains, microstructure and magnetic properties of highly oriented barium ferrite thin films with perpendicular anisotropy have been investigated with magnetic force microscopy (MFM), VSM, SEM and TEM. Two kinds of magnetic domain are energetically favourable: (a) cluster-like structure in as-deposited films grown at 770 °C; (b) stripe domains in layers annealed at high temperature (900 °C). Such a difference in domain configuration can be related to microstructure. Small single-domain grains (70 nm) exist in as-deposited films whereas annealed films consist of large multidomain platelets. The magnetic measurements (hysteresis loops and virgin curves) reveal that magnetization reverses by rotation and wall motion for cluster-like and stripe domains respectively. A good agreement was established between the domain width measured by MFM and that predicted by using the Kooy–Enz model (Kooy C and Enz U 1960 *Philips Res. Rep.* **15** 7) in our stripe structure. The analyses of minor loops and virgin curves suggest that the coercivity in stripe domains is controlled by wall nucleation rather than pinning.

1. Introduction

Magnetic thin films with perpendicular anisotropy are of great interest for fundamental studies as well as for applied research. Potential applications of these films include magneto-optic and perpendicular magnetic recording. Generally the orientation of the easy axis results from the competition between various kinds of magnetic anisotropy in the media. In thin films [1–3], perpendicular anisotropy can be achieved only if the shape anisotropy is overcome by other sources of anisotropy such as magnetocrystalline and stress. However in ultra-thin films [4–7] and multilayers [8, 9], the interface anisotropy prevails and can stabilize the easy axis out of plane.

[3] Author to whom any correspondence should be addressed.

Barium ferrite ($BaFe_{12}O_{19}$) material is a magnetic oxide with hexagonal structure and seems to be a potential candidate for magnetic as well as magneto-optic recording. Beside its high chemical stability and mechanical hardness, $BaFe_{12}O_{19}$ exhibits a large magnetocrystalline anisotropy, which can offer a double benefit.

(a) A perpendicular anisotropy can be easily achieved in thin films.
(b) A reduction of the grain size is possible while retaining a stable magnetization (6.7 nm is the superparamagnetic limit size), which constitutes an important requirement for application in high-density magnetic recording.

Additionally $BaFe_{12}O_{19}$ exhibits a large Kerr rotation in the UV wavelength [10], related to the charge transfer transitions in tetrahedral and octahedral sites of Fe^{3+}. Many studies have reported on magnetic properties of $BaFe_{12}O_{19}$ thin films grown with different techniques on various substrates such as Al_2O_3, SiO_2/Si and fused quartz buffered with ZnO layer [11–14]. However sapphire substrate is more attractive because it can ensure an epitaxial growth [11] due to its rhombohedral structure on which hexagonal barium ferrite can fit. On the other hand, Al_2O_3 can support high temperatures without any diffusion toward the $BaFe_{12}O_{19}$ layer.

The first important investigations of $BaFe_{12}O_{19}$ magnetic domains have been performed on a bulk single crystal [15]. By using the Faraday technique, Kooy and Enz succeeded in imaging magnetic domains in platelets 3 μm thick. Despite the advantage of imaging under applied magnetic field, the resolution of this magneto-optic technique is limited to 300 nm. However due to low thickness in thin-film media, magnetic domains are expected to be small and cannot be resolved by this technique. The development of new imaging techniques such as magnetic force microscopy (MFM) has shown very promising results in the investigation of domain structure in thin films [16–18]. Based on the interaction between the magnetic tip and the sample, the stray field can be imaged with quite high resolution. Moreover MFM is a very powerful tool with which to study magnetic coupling because both topography and magnetic domains can be imaged.

In this paper we applied MFM to investigate the structure of magnetic domains in highly oriented $BaFe_{12}O_{19}$ thin films. Our study was performed on as-deposited films grown at 770 °C as well as on samples annealed at temperatures up to 900 °C.

2. Experimental technique and conditions of the film growth

The $BaFe_{12}O_{19}$ samples have been prepared with pulsed laser deposition (PLD). The setup of this technique consists of a laser, vacuum chamber, $BaFe_{12}O_{19}$ target and substrate directly in contact with the heater. Before every deposition, the vacuum chamber was evacuated down to base pressure (2×10^{-7} mbar) with a turbo-molecular pump. The KrF excimer laser operates in the UV and delivers a beam (248 nm wavelength and 23 ns pulse width) which is focused with a lens on the barium ferrite target. During ablation the $BaFe_{12}O_{19}$ target was rotated with a motor to ensure its uniform wear. (001) sapphire with one polished side has been used as growth substrate. The output energy of the laser and the position of the lens were adjusted to ablate with a 1.5 J cm^{-2} energy density. The distance between the target and substrate and the laser repetition have been kept constant at 45 mm and 5 Hz respectively. During deposition O_2 was supplied in order to achieve stoichiometric films. Moreover, before each growth, the target was pre-ablated for 5 min. Two kinds of sample have been prepared.

(1) Sample A is a film grown at high temperature (770 °C).
(2) Sample B was prepared in two different steps: (a) deposition at relatively low substrate temperature (620 °C) and 50 mTorr of oxygen pressure and (b) successive annealing at temperatures from 640 to 900 °C with a step of 20 °C.

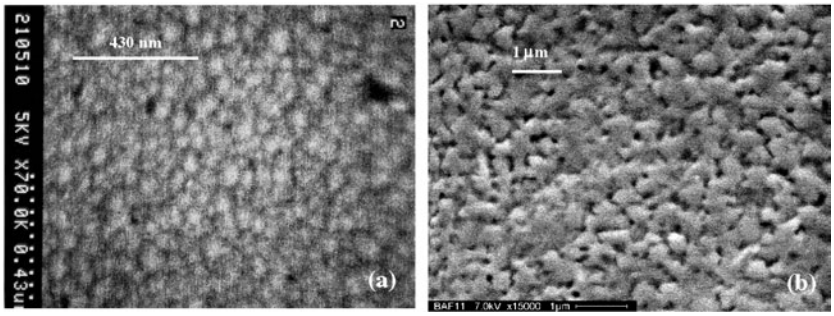

Figure 1. SEM images of (a) as-grown film (A) at 770 °C showing a granular structure and (b) annealed sample (B) at 900 °C with large platelets.

The annealing process was performed in an oven in an O_2 atmosphere for 1 h at each temperature. Other films have been prepared under similar conditions to sample A (770 °C), but in different O_2 pressures (20–500 mTorr). It was established that microstructure and magnetic properties of the films are less sensitive to O_2 pressure than deposition temperature and film thickness.

3. Structural analyses

A SEM image of sample A (300 nm thick) is shown in figure 1(a). The film exhibits a very smooth surface and its morphology consists of a granular structure with homogeneous size distribution. The grains possess a circular shape with 70 nm as mean diameter. Figure 1(b) is a SEM picture of sample B (300 nm thick). As mentioned before, sample B was the subject of thermal annealing at successive temperatures up to 900 °C. It is important to point out that before the annealing process, film B was poorly crystallized even though grown at the relatively high temperature of 620 °C. From figure 1(b) the structure of the film seems to be more continuous and its topography consists of platelets well connected to each other. In contrast to figure 1(a), the platelet size is not uniform and exceeds 500 nm. XRD measurements ($\theta/2\theta$ scan) performed on both samples reveal a single $BaFe_{12}O_{19}$ phase and a high crystallographic orientation parallel to the (001) texture. To estimate the c-axis dispersion, rocking curves of both films have been measured. As shown in figure 2 film (A) exhibits a very narrow angular distribution of c-axis with a small dispersion (0.5°) as indicated by the full width at half maximum (FWHM). However sample (B) annealed at 900 °C shows a more dispersed c-axis (1.5°) as confirmed by the width of the rocking curve.

In order to study the quality of growth, a TEM cross-section of a film grown under similar conditions to sample A (770 °C and 50 mTorr of O_2 pressure) is presented in figure 3. Even though grown at a high deposition temperature, the interface between Al_2O_3 substrate and $BaFe_{12}O_{19}$ film is well defined with no interdiffusion being observed in this region. However the film exhibits an epitaxial growth with some dislocations and non uniform structure from the top to interface. The dislocations are certainly caused by the stress due to the misfit between the rhombohedral structure of Al_2O_3 ($a = 0.5128$ nm) and the hexagonal lattice of $BaFe_{12}O_{19}$ ($a = 0.588$ nm). It was reported that matching between both lattices could be realized in two different configurations [19]. However, the dislocations are necessary to minimize the growth energy to keep a relaxed lattice at the top of the film as shown in the image of figure 3.

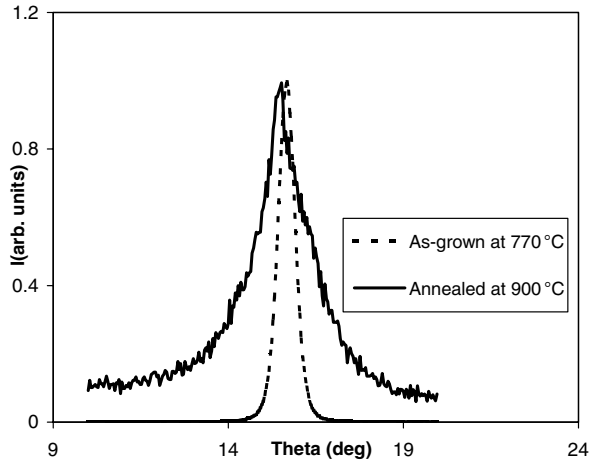

Figure 2. XRD rocking curves of as-grown and annealed films, measured at the (008) peak. The FWHM indicates a more dispersed *c*-axis in the sample annealed at 900 °C.

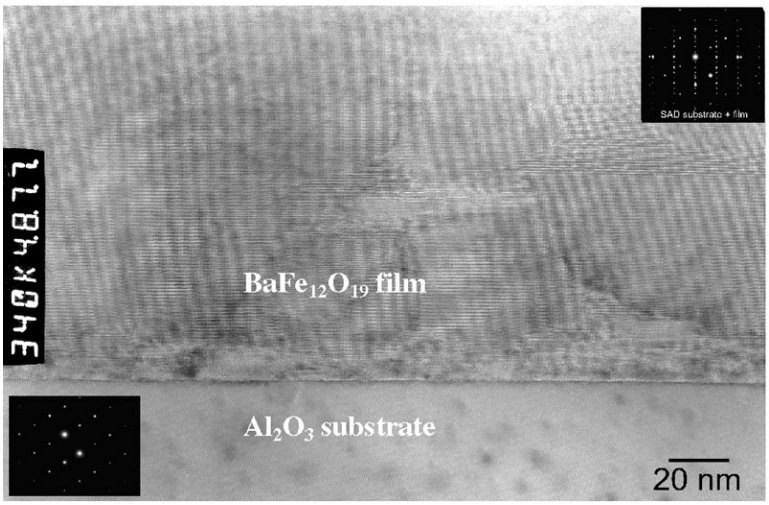

Figure 3. TEM cross-section of as-grown film at 770 °C. The image exhibits an epitaxial structure with some dislocations.

4. Magnetic properties

Due to the importance of microstructure in magnetism, one priority of this study was to correlate the structures of films to their magnetic properties and to establish the annealing effects. Figure 4 shows hysteresis loops of sample A measured by VSM with the applied field parallel and perpendicular to the film plane respectively. The perpendicular loop exhibits a considerable hysteresis with a 200 kA m^{-1} coercivity and a remanence close to 0.6. One source of squareness reduction is the demagnetizing field, which induces a shearing in the loop. However the in-plane loop exhibits a linear behaviour and saturates around 1300 kA m^{-1}, which is close to the single-crystal anisotropy field ($H_k = 2K_u/M_s = 1380$ kA m^{-1}, $K_u = 0.33 \times 10^6$ J m^{-3} and $M_s = 380$ kA m^{-1} are the anisotropy constant and magnetization respectively of the single

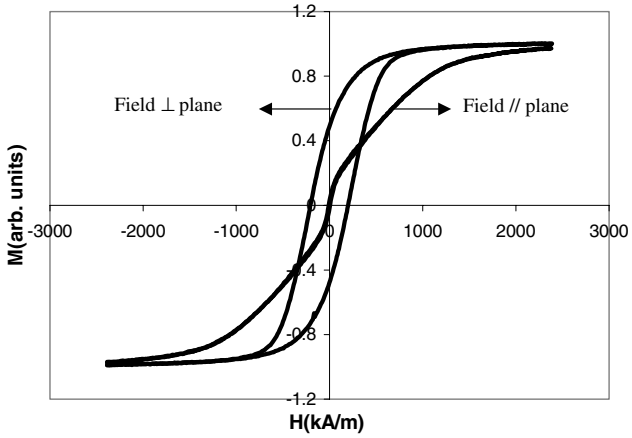

Figure 4. In-plane and perpendicular magnetization loops showing a full perpendicular anisotropy in as-deposited film at 770 °C.

crystal). With a simple comparison between both loops, it is easier to confirm the perpendicular orientation of magnetic anisotropy in this film. The anisotropy constant and the magnetization were measured with torque and VSM methods respectively and were estimated to be 80% of the bulk values. It is interesting to point out the large difference between the coercivity ($H_c = 200$ kA m^{-1}) and the effective anisotropy field ($H_{keff} = H_k - M_s = 1000$ kA m^{-1}) in film A. This difference may be due to the mode of magnetization reversal. Angular studies of coercivity and remanence coercivity as well as analysis of rotational hysteresis revealed that curling seems to be an appropriated mode for magnetization reversal in such a structure [20]. One crucial parameter in the control of magnetization reversal is the microstructure, which in our case seems to favour an incoherent rotation mode (circular grains with large size (70 nm)). Another probable source of reduction of coercivity is the exchange coupling between grains, which will be discussed in the next section.

In order to characterize film B, it is important to investigate the different changes in magnetic properties, which arise during the annealing process. Before annealing, sample B was not magnetic even though grown at a relatively high deposition temperature (620 °C). No hysteresis was observed in either in-plane or perpendicular directions. This could be explained by the amorphous structure of the sample. It is important to mention that in barium ferrite material, magnetic properties such as anisotropy and magnetization are induced by a local order, where Fe^{3+} sites play a very important role. As shown in figure 5, at the first stage of annealing (660 °C) film B exhibits a weak magnetization with a fully perpendicular easy axis. By increasing annealing temperature, figure 5 reveals through the in-plane and perpendicular magnetization loops that many effects occurred that can be summarized as follows.

- The magnetic moment increases with huge change between 700 and 760 °C. Above 760 °C, the magnetic moment is more or less constant, indicating a full crystallization of the material.
- With increasing annealing temperature, the coercivity of the perpendicular loop drops drastically to become constant above 760 °C ($H_c = 50$ kA m^{-1}). The reduction in coercivity is probably due to the large change in size of grains, which finally form large platelets well connected to each other (see figure 1(b)). Due to their dimensions the platelets cannot remain as single domains but a multidomain state becomes energetically favourable as revealed by the MFM study of the next section.

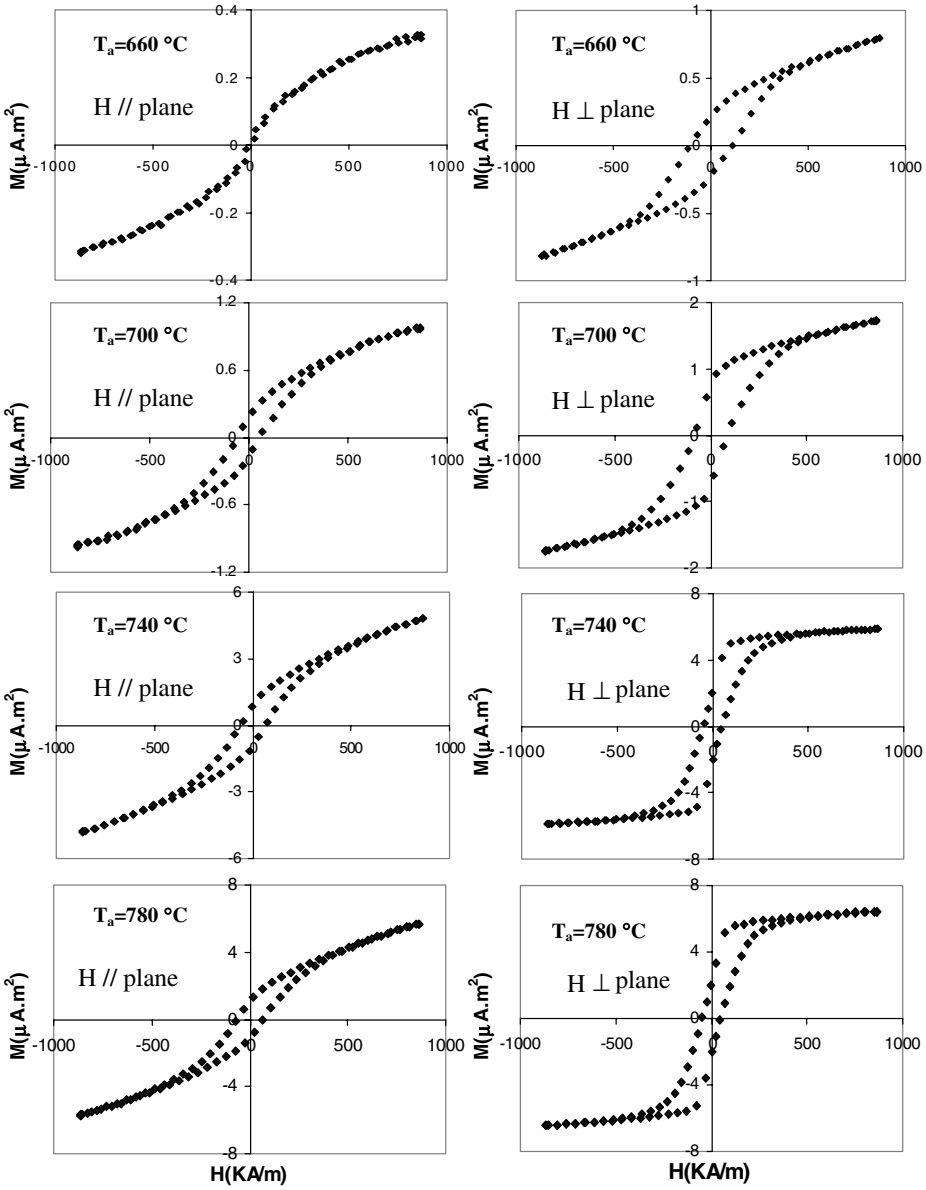

Figure 5. In-plane (left) and perpendicular (right) loops measured after successive annealing at temperatures between 660 and 780 °C. The film was initially deposited at 620 °C.

- In-plane magnetization arises as indicated by the large hysteresis of in-plane loops. This may have two possible origins. (1) Some misorientations of crystals, which can induce an in-plane magnetization. In addition to strong (00l) reflections, a $\theta/2\theta$ scan reveals the existence of a small (107) peak. Such texture indicates that the c-axis is tilted about 61° from the film plane and can induce an in-plane hysteresis. (2) The stress anisotropy caused by the mismatch between the $BaFe_{12}O_{19}$ lattice and that of Al_2O_3 [21]. This misfit is expected to increase with annealing temperature due to the difference in thermal expansion of these two materials. A good argument supporting the existence of stress is

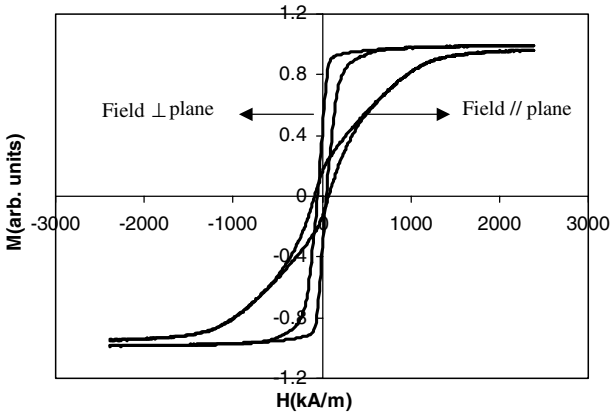

Figure 6. In-plane and perpendicular magnetization loops after annealing at 900 °C. The film shows a low coercivity ($H_c = 50$ kA m^{-1}) and a large in-plane hysteresis.

clearly shown in our recent magneto-optic study [22]. The result indicates a significant difference in magnetization loops measured with Kerr and VSM methods respectively. However the Kerr loop with its large coercivity is a direct measurement of the top of the $BaFe_{12}O_{19}$ layer (about 15 nm), where the lattice is supposed to be more relaxed. In contrast to the Kerr method, VSM estimates the average magnetization in the whole sample. The low coercivity measured by VSM in comparison to the Kerr method reveals that magnetic properties are not uniform from the top to the film interface. This could be explained by stress, which is expected to be stronger at the interface.

- The switching field distribution illustrated by the magnetization slope at the coercive field becomes narrow with increasing annealing temperature. Moreover the nucleation field corresponding to the singularity point in the magnetization loop is better defined at high annealing temperatures.

Magnetic properties of the highest annealing temperature (900 °C) are illustrated in the two loops measured with a large maximum field (2387 kA m^{-1}) (figure 6). The perpendicular loop exhibits a low coercivity (50 kA m^{-1}) and very well defined nucleation field. It is important to point out that the main changes in magnetic properties of sample B occurred at annealing temperatures below 760 °C and nothing happened above this temperature. Such a result suggests the possibility of a direct comparison between magnetic properties of film A (as grown at 770 °C) and those of film B (annealed at 900 °C). As shown in the loops of film A, the coercivity is quite large (200 kA m^{-1}) and the magnetization reversal is smoother (figure 4), indicating a broad nucleation field distribution. It is not surprising to see a significant difference in the structure of magnetic domains in both samples (A and B) due to the large difference in coercivities and nucleation fields. The in-plane loop of film B (figure 6) shows a large hysteresis, which is mainly due to crystal misorientations and stress. However the smoothness in saturation of in-plane loop indicates a certain dispersion in the anisotropy field. This dispersion may be explained as follows: in the region close to the interface, the lattice of $BaFe_{12}O_{19}$ is the subject of a large stress, which deforms the a-axis. This stress will reduce the effective anisotropy field, due to its in-plane anisotropy, whereas magnetocrystalline anisotropy is perpendicular. However at the top of the film where the lattice is more relaxed, the origin of anisotropy is mainly magnetocrystalline.

An interesting result, which clearly illustrates the large difference in the magnetization process of as-grown film at 770 °C (A) and that annealed at 900 °C (B) is presented in figure 7.

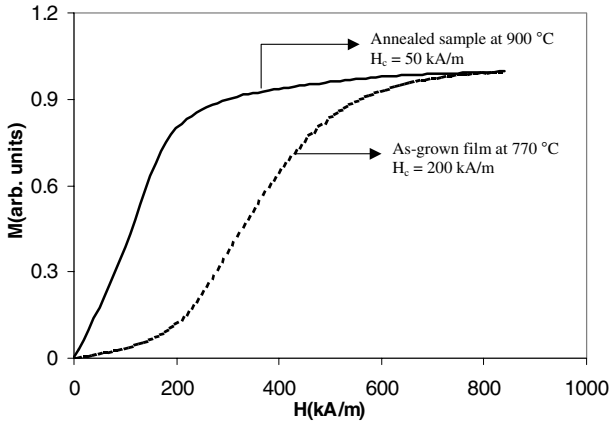

Figure 7. Virgin curves of both films (as-deposited A and annealed B). Annealed sample exhibits a high initial susceptibility and fast magnetization increase at low fields.

The behaviour of both virgin curves deviates strongly from each other, especially at low field. The slope of the virgin curve at zero field is a direct measurement of the initial susceptibility (χ). χ is very large in the annealed film (B) despite the shearing due to the demagnetizing effect, whereas it is close to zero in the as-grown film. This huge difference in magnetic properties is certainly related to the mode of magnetization reversal, which is discussed in more detail in the next section. In fact film B exhibits multidomain platelets favourable to wall motion. However the as-grown film (A) possesses small single-domain grains where the magnetization can reverse by an incoherent rotation mode.

5. Structure of magnetic domains

A commercial MFM (Digital Instruments, DI 3100) was applied to study the structure of domains in our $BaFe_{12}O_{19}$ films. Both topography and magnetic structure have been imaged using the tapping-lift mode. In such measurements every line is scanned twice under the same conditions; only the height of the magnetic tip is different. In the first scan, the topography is imaged with the tapping mode. However, in the second scan, after being removed a certain height from the surface, the magnetic tip becomes sensitive mainly to magnetic forces allowing the image of the stray field of the sample. The gradient of magnetic force induces a shift in the vibration frequency of the cantilever, which is detected as the feedback control signal. In all measurements, we used a commercial Si tip coated with a CoCr thin film (30 nm). The tip was vertically magnetized and its lift height was fixed at 70 nm during the scan of the magnetic image. In figure 8, we present 2 μm $\times$ 2 μm AFM and MFM pictures of barium ferrite film prepared in similar conditions to sample A. Magnetic properties of this film are shown in figure 4. The AFM image (figure 8(a)) agrees with SEM measurements (circular grains close to each other). The MFM picture (figure 8(b)) is of the sample in an ac demagnetized state. Due to the high perpendicular anisotropy of the film, there is only one way for the magnetization to minimize magnetostatic energy by choosing up and down as directions. The magnetic image (figure 8(b)) consists of a domain pattern with a cluster-like structure with up and down magnetization corresponding to dark and white contrast respectively. It is clear that each cluster-like domain contains many coupled grains. In contrast to the homogeneous size distribution of grains, there is a large dispersion in size as well as in shape of magnetic domains. In figure 9 the topography and domain pattern of sample B are shown. The magnetic image corresponds to the ac demagnetized state of the film and consists of stripe domains

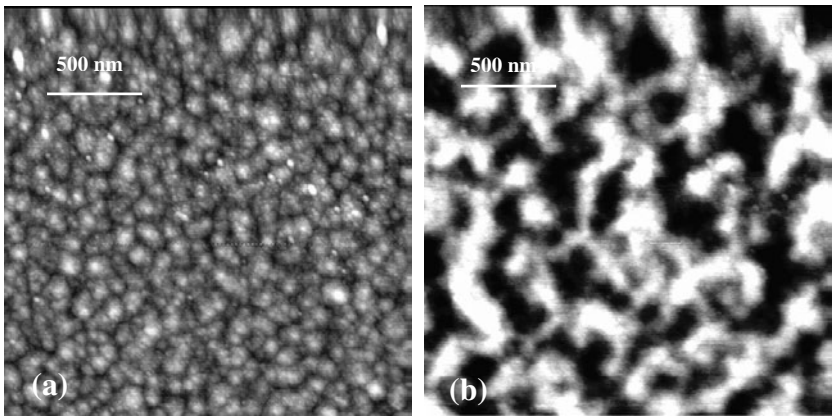

Figure 8. (2 μm $\times$ 2 μm) (a) AFM and (b) MFM images of as-grown film at 770 °C showing granular microstructure with cluster-like domains with up (dark contrast) and down (white contrast) magnetization. Note the piezo drift at the top of the images.

with up and down magnetization (dark and white contrast respectively). The average width of magnetic domains in this stripe structure was estimated to be 350 nm. It is important to point out that the large difference between the domain structure in as-grown film (cluster-like domain in figure 8(b)) and annealed sample at 900 °C (stripe structure of figure 9(b)) is mainly due to microstructure. The AFM and SEM pictures of annealed film (figures 1(b) and 9(a)) reveal a more continuous morphology with very big platelets close to each other, whereas the topography of as-grown film (figures 1(a) and 8(a)) looks more granular (70 nm circular grains). With this large difference in size and morphology, it is not surprising to see a change in domain structure. One important parameter that controls the size and structure of magnetic domains is the exchange coupling, which seems to be at least uniform in one platelet (1 μm or more) in annealed $BaFe_{12}O_{19}$ film. However the long range of uniformity of exchange coupling is certainly reduced in the as-grown sample with relatively small circular grains (70 nm). Another important point concerns the magnetic state of the grain and that of the platelet. As clearly shown in figure 8 one grain in as-deposited film is always single domain (many coupled grains constitute one domain). However the topography and magnetic structure of figure 9 reveal that one platelet possesses multidomains. According to Zijlstra [23], the critical diameter for the existence of a spherical single-domain particle is given by $d_c = 72(AK_u)^{1/2}/\mu_0 M_s^2$. M_s is the particle magnetization, K_u is the uniaxial anisotropy constant and A is the exchange energy. By introducing the parameters of single-crystal barium ferrite ($M_s = 380\,\mathrm{kA\,m^{-1}}$, $A = 1.7 \times 10^{-11}\,\mathrm{J\,m^{-1}}$, $K_u = 3.3\times10^5\,\mathrm{J\,m^{-3}}$) d_c is estimated at 1 μm. Due to the contribution of the shape anisotropy in our case, d_c is expected to be much smaller than that predicted by Zijlstra [23].

The first stripe structure was reported by Kooy and Enz [15] in bulk single-crystal barium ferrite. By using the Faraday technique, the magnetic structure was imaged and the domain width was measured as a function of applied field. In their study, Kooy and Enz showed that the field dependence of domain width exhibits two regimes. At low fields, the sum of the widths of the domains parallel and antiparallel to the field is more or less constant. At large fields, the size of the domain parallel to the field shows a very fast increase, whereas that of the reversed domain decreases slowly. Another remarkable result of their work concerns the behaviour of the reversed domain at large fields close to saturation. It was reported that saturation does not take place by reducing the width of the reversed domain to zero, but by a reduction of its length and a contraction towards a cylindrical shape. A simple comparison between our result and that of Kooy and Enz allows us to conclude that our stripe domain structure resembles

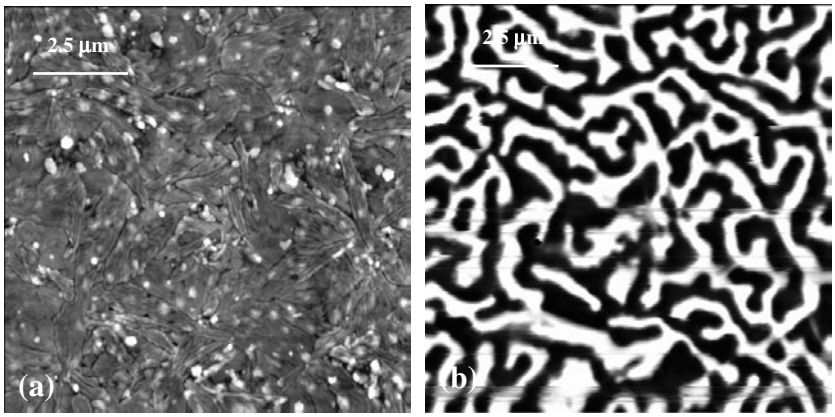

Figure 9. 10 μm $\times$ 10 μm (a) AFM and (b) MFM images of film annealed at 900 °C. The film structure consists of platelets with stripe domains.

that observed in a $BaFe_{12}O_{19}$ single crystal. We can confirm that annealing creates a structure with big platelets approaching the single-crystal behaviour. Despite the existence of similar stripe domains in our film (figure 9(b)) and a single crystal [15], magnetic properties in both structures show a significant disagreement. The coercivity in our annealed layer is quite large ($H_c = 50$ kA m^{-1}) (figure 6) whereas H_c is close to zero in the single-crystal structure. Additionally the shoulder in the hysteresis loop of the bulk [15] is much more pronounced than in our case. The large coercivity in our film (sample B) could be explained by the existence of a lot of boundaries and defects between the platelets. The existence of the shoulder in the loop of a system with perpendicular anisotropy is related to domain nucleation and can be well understood in the model developed by Cape and Lehman [24]. It was shown that by reducing the field from saturation state, one or more nucleation centres appear to give birth to magnetic domains, which spread over the whole sample [15]. These nucleation centres are probably induced by imperfections in the system. Consequently, it is not surprising that the nucleation process is different in our case due to the polycrystalline structure with large defects. Another interesting work, which supports our results, is published in [25, 26]. The latter study was performed on Co–Cr films with perpendicular easy axis. The magnetocrystalline anisotropy and shape of columns are the main sources of magnetic anisotropy in such films. With polar Kerr microscopy, Lodder *et al* [25, 26] succeeded in imaging the domain structure under various applied fields. Two kinds of magnetic domain have been identified and were classified as follows.

(1) Stripe domains exist only for a system with low coercivity and hysteresis loop with a well defined shoulder.
(2) Domains with cluster-like structure are more favourable in a layer with large coercivity and without any shoulder.

In order to study the magnetization reversal in our film with stripe domains, we performed further imaging of the sample in different magnetization states. Figure 10 shows an MFM picture of the annealed sample in the remanence state. This state was reached by applying first a large field parallel to the easy axis and enough to saturate the magnetization. In the second step, the field was reduced to zero for the MFM measurement. The magnetic image of figure 10 consists of bubbles with an elliptical shape and non-uniform size. These bubbles exhibit an opposite magnetization to that of the fully saturated state. However, the first stage of the formation of the bubbles starts around the singularity point in the magnetization loop

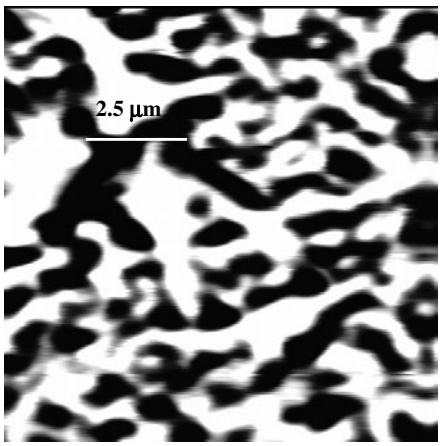

Figure 10. Structure of magnetic domains of annealed film at 900 °C imaged in the remanent state after saturation with large field parallel to the easy axis. Elongated bubbles exist and are randomly oriented.

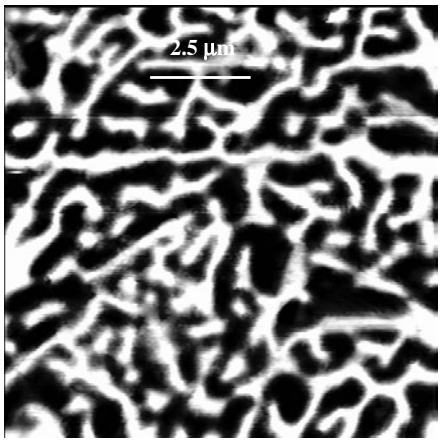

Figure 11. ($10\,\mu$m $\times$ $10\,\mu$m) MFM picture imaged in the dc demagnetized state showing random stripe domains.

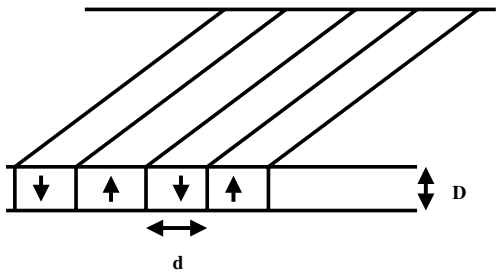

Figure 12. Distribution of magnetic domains in demagnetized state of a system with perpendicular anisotropy.

(nucleation field). It was reported by Thiele [27] that during their growth magnetic bubbles adopt an elliptical shape, which seems to agree with our result. In the same state (remanence), a similar structure was observed in our recent work performed on Co thin films obliquely sputtered on polymer [28] as well as in the study of Hehn *et al* [17] on Co epitaxially grown on sapphire. Moreover bubbles in our Co thin films [28] were found to grow in an interesting way in which the elliptic shape stays parallel to the longitudinal direction. This behaviour was explained by the tilt of the easy axis and the existence of an in-plane uniaxial anisotropy confined to the longitudinal direction. It is interesting to point out that due to low remanence in single-crystal barium ferrite no bubble structure was reported in the study of Kooy and Enz [15]. Nevertheless, straight stripe domains were found to be energetically favourable in the latter structure. In figure 11, we present an MFM picture of sample B, imaged in the dc demagnetized state. This method of demagnetization consists of two steps.

(a) Saturation with a large field parallel to the easy axis.
(b) The field is reversed to a value called the remanence coercivity ($H_r = 99$ kA m^{-1}) then removed.

The magnetic image of figure 11 consists of stripe domains and resembles that of the sample in an ac demagnetized state (figure 9). The magnetic state of figure 11 seems to be a continuation of the structure observed at remanence (figure 10). By decreasing the field from 0 to $-H_r$ magnetic bubbles grow and coalesce to form stripe domains as shown in figure 11.

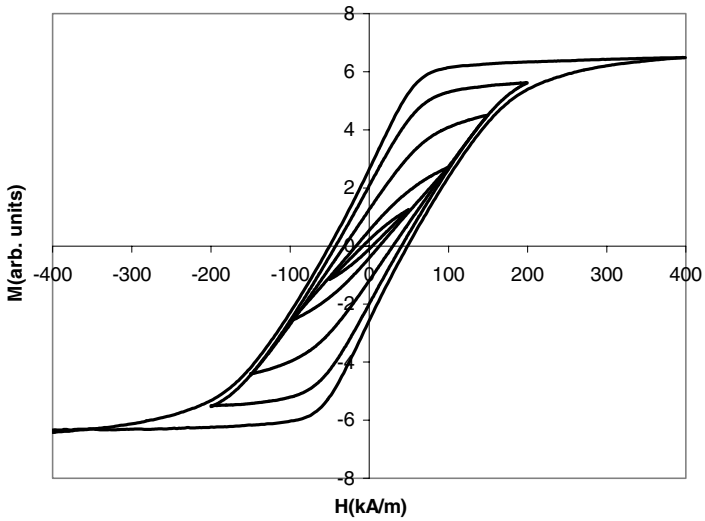

Figure 13. Minor loops of annealed film at 900 °C measured with maximum applied field between 10 and 400 kA m^{-1}.

It is important to point out that the Kooy–Enz model [15] originally built for a single crystal fits well to the experimental results. It will be interesting to test the applicability of such a model to our polycrystalline film in order to estimate the width of our stripe domains. In their model, Kooy and Enz consider a uniform magnetization and a perpendicular anisotropy in the bulk platelet. If the sample is demagnetized, the distribution of the magnetization consists of up and down with equal widths as shown in figure 12. In this model, the total energy of the system has two sources, which are wall and magnetostatic energies. The wall energy per surface unit is given by $E_w = \sigma_w D/d$; σ_w is the specific wall energy, d is the domain width and D is the layer thickness. The magnetostatic energy is given by this formula:

$$E_d = (32M_s^2 d/\pi^2)(1+\sqrt{\mu})\sum_{k=0}^{\infty}(1-\exp(-\pi(2k+1)D\sqrt{\mu}/d))/(2k+1)^3$$

where M_s is the layer magnetization, $\mu = 1 + 2\pi M_s^2/K_u$ and K_u is the uniaxial anisotropy constant.

By minimizing the total energy with the parameters of our barium ferrite layer ($\sigma_w = 9.47 \times 10^{-3}$ J m^{-2}, $2\pi M_s^2 = 0.8 \times 10^5$ J m^{-3}, D=300 nm, $K_u = 2.5 \times 10^5$ J m^{-3}), the domain width was estimated to be 380 nm. Such a width value shows a good agreement with that measured by MFM (350 nm).

An important question arises: what kind of mechanism is involved in the control of coercivity in our film with stripe structure? It is well known in permanent magnets such as NdFeB and SmCo that the mechanism of magnetization reversal is governed by wall nucleation and pinning depending on the microstructure and material preparation [29–33]. Many effects established in a film with stripe domains (sample B) such as low coercivity ($H_c = 50$ kA m^{-1}), existence of platelets with multidomain structure and the behaviour of the virgin curve suggest that the wall has an important role in the magnetization process. Now the crucial question is: what is the wall behaviour in such media? In order to discriminate between the two mechanisms (nucleation and pinning) in our material, we performed analyses of minor loops. In this experiment, the field was applied parallel to the easy axis and the sample was ac demagnetized before each minor loop measurement. Figure 13 shows the behaviour of minor loops measured

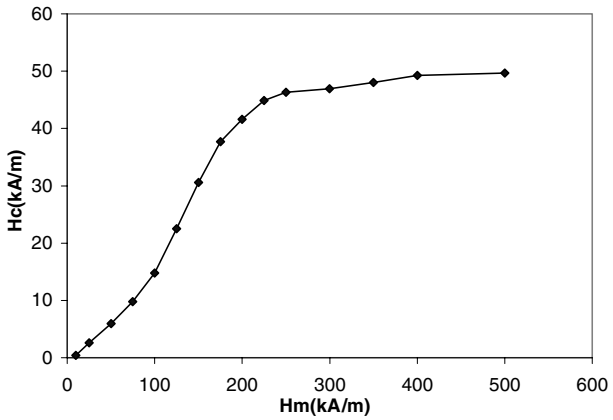

Figure 14. Coercivity dependence on maximum applied field. The shape of this curve reveals that the coercivity is likely to be wall nucleation controlled.

under different maximum applied fields up to 400 kA m^{-1}. Increasing the maximum applied field induces a drastic change in the minor loop that can be summarized as follows.

(a) A reduction in the shearing of the minor loop.
(b) The coercivity, the remanent magnetic moment and the slope at the coercivity increase to saturate at the major loop.

The shape of our minor loops (figure 13) deviates strongly from that measured by Speliotis [34] in oriented particulate barium ferrite. In his study, Speliotis showed that by reducing the maximum applied field, the minor loop exhibits a small change from the major loop until the maximum applied field becomes close to the coercivity. Moreover no significant change was observed in the remanent magnetic moment. Such a large disagreement with our result could be related to microstructure. It is important to point out that samples used in the Speliotis study consist of very small single-domain platelets, where magnetization reversal is likely to be a rotation, whereas our film exhibits big multidomain platelets favourable to wall motion. Figure 14 shows the dependence of coercivity of the minor loop on maximum applied field. At low fields, the coercivity exhibits a fast increase with a fairly constant slope. However at large fields, the coercivity saturates above 250 kA m^{-1}. Such behaviour is typically characteristic of wall nucleation rather than pinning where the coercivity exhibits three regimes following the maximum applied field. The three steps in the pinning process consist of the following.

(a) Very small change in coercivity at low fields.
(b) A huge increase in H_c occurs above a critical field (pinning field).
(c) H_c saturates at large field.

The wall nucleation is conceivable in our film because at least two strong arguments, which are the shape of the virgin curve with high initial susceptibility (figure 7) and the coercivity of minor loops (figure 14), support this hypothesis. The wall nucleation supposes the existence of nucleation centres. Despite the single-crystal structure of the bulk platelet, it was reported by Kooy and Enz [15] that the wall nucleates from many centres to spread in the whole sample. These nucleation centres are believed to be some imperfections in the crystal. In our case the nucleation centres could be the grain boundaries as well as defects in the multidomain platelets.

6. Conclusions

The microstructure, magnetic properties and structure of magnetic domains in highly oriented $BaFe_{12}O_{19}$ films with perpendicular anisotropy were investigated by different analyses such

as MFM, VSM, SEM, TEM and XRD. Two kinds of magnetic domain were found to be energetically favourable. Films grown at 770 °C show domains with a cluster-like structure, whereas annealed sample at 900 °C exhibits stripe domains. The difference in the domain configuration has been related to the microstructure. It was established that as-deposited films (770 °C) consist of granular structure with small single-domain grains (70 nm). However in annealed films, the microstructure and magnetic image reveal the existence of big platelets with a multidomain structure. The analyses of minor loops and virgin curves support the hypothesis of wall nucleation in the stripe structure. A good agreement exists between the domain width measured by MFM (350 nm) and that predicted by the Kooy–Enz model (380 nm).

Acknowledgment

The authors would like to thank Dr G N Phillips for his helpful comments.

References

[1] Cebollada A *et al* 1994 *Phys. Rev.* B **50** 3419
[2] Lairson B M, Visokay M R, Sinclair R and Clemens M B M 1993 *Appl. Phys. Lett.* **62** 639
[3] Masterson H J *et al* 1993 *J. Appl. Phys.* **73** 3917
[4] Allenspach R, Stampanoni M and Bischof A 1990 *Phys. Rev. Lett.* **65** 3344
[5] Pommier J, Meyer P, Penissard G, Ferre J, Bruno P and Renard D 1990 *Phys. Rev. Lett.* **65** 2054
[6] Thomassen J *et al* 1992 *Phys. Rev. Lett.* **69** 3831
[7] Qiu Z Q, Pearson J and Bader S D 1993 *Phys. Rev. Lett.* **70** 1006
[8] Carcia P F, Meinhaldt A D and Suna A 1985 *Appl. Phys. Lett.* **47** 178
[9] Nakajima N *et al* 1998 *Phys. Rev. Lett.* **81** 5229
[10] Lisfi A, Lodder J C, de Haan P, Haast M A M and Roesthuis F J G 1998 *J. Mag. Soc. Japan* (Suppl. S2) **22** 159
[11] Yuan M S, Glass H L and Adkins L R 1988 *Appl. Phys. Lett.* **53** 340
[12] Xiaoyn Sui and Kryder M H 1993 *Appl. Phys. Lett.* **63** 1582
[13] Lisfi A, Lodder J C, de Haan P, Smithers M A and Roesthuis F J G 1998 *IEEE Trans. Magn.* **34** 1654
[14] Dorsey P C and Vittoria C 1994 *J. Magn. Magn. Mater.* **137** 89
[15] Kooy C and Enz U 1960 *Philips Res. Rep.* **15** 7
[16] Bochi G, Hug H J, Paul D I, Stiefel B, Moser A, Parashikov I, Guntherodt H-J and O'Handley R C 1995 *Phys. Rev. Lett.* **75** 1839
[17] Hehn, M, Padovani S, Ounadjela K and Bucher J P 1996 *Phys. Rev.* B **54** 3428
[18] Gehanno V, Marty A, Gilles B and Samson Y 1997 *Phys. Rev.* B **55** 12552
[19] Shinde S R, Ramesh R, Lofland S E, Bhagat S M, Ogale S B, Sharma R P and Venkatesan T 1998 *Appl. Phys. Lett.* **72** 3443
[20] Lisfi A and Lodder J C 1999 *IEEE Trans. Magn.* **35** 2754
[21] Wyckoff R W G 1964 *Crystal Structures* vol 2, 2nd edn (New York: Wiley–Interscience) p 6
Wyckoff R W G 1965 *Crystal Structures* vol 3, 2nd edn (New York: Wiley–Interscience) p 497
[22] Lisfi A and Lodder J C 2002 at press
[23] Zijlstra H 1982 *Ferromagnetic Materials: a Handbook on the Properties of Magnetically Ordered Substances* vol 3, ed E P Wohlfarth (Amsterdam: North-Holland)
[24] Cape J A and Lehman G W 1971 *J. Appl. Phys.* **42** 5732
[25] Lodder J C, Wind D, Dorssen G E V, Popma Th J A and Hubert A 1987 *IEEE Trans. Magn.* **23** 214
[26] Lodder J C, Wind D, Popma Th J A and Hubert A 1987 *IEEE Trans. Magn.* **23** 2055
[27] Thiele A A 1971 *Bell Syst. Tech. J.* **50** 725
[28] Lisfi A and Lodder J C 2001 *Phys. Rev.* B **63** 174441
[29] Buschow K H J 1986 *Mater. Sci. Rep.* **1** 1
[30] Hadjipanayis G C and Kim A 1988 *J. Appl. Phys.* **63** 3310
[31] Herbst J F 1991 *Rev. Mod. Phys.* **63** 819
[32] Kronmuller H, Durst K-D and Sagawa M 1988 *J. Magn. Magn. Mater.* **74** 291
[33] Livingston J D 1986 Soft and Hard Magnetic Materials with Applications *Am. Soc. Met. Symp. Proc.* (Metals Park, OH: American Society for Metals) p 71
[34] Speliotis D E 1987 *IEEE Trans. Magn.* **23** 3143